



HAL
open science

On the return to isotropy from anisotropic homogeneous turbulent shear flow

Frank G Jacobitz, Kai Schneider

► **To cite this version:**

Frank G Jacobitz, Kai Schneider. On the return to isotropy from anisotropic homogeneous turbulent shear flow. 13th International Symposium on Turbulence and Shear Flow Phenomena (TSFP13) Montreal, Canada, June 25–28, 2024, Jun 2024, Montréal, Canada. hal-04597151

HAL Id: hal-04597151

<https://hal.science/hal-04597151>

Submitted on 1 Jun 2024

HAL is a multi-disciplinary open access archive for the deposit and dissemination of scientific research documents, whether they are published or not. The documents may come from teaching and research institutions in France or abroad, or from public or private research centers.

L'archive ouverte pluridisciplinaire **HAL**, est destinée au dépôt et à la diffusion de documents scientifiques de niveau recherche, publiés ou non, émanant des établissements d'enseignement et de recherche français ou étrangers, des laboratoires publics ou privés.

ON THE RETURN TO ISOTROPY FROM ANISOTROPIC HOMOGENEOUS TURBULENT SHEAR FLOW

Frank G. Jacobitz

Department of Mechanical Engineering, University of San Diego
5998 Alcalá Park, San Diego, CA 92110, USA
jacobitz@sandiego.edu

Kai Schneider

Institut de Mathématiques de Marseille (I2M), Aix-Marseille Université, CNRS
3 place Victor Hugo, case 19, 13331 Marseille Cedex 3, France
kai.schneider@univ-amu.fr

ABSTRACT

This contribution presents direct numerical simulation results on the anisotropy properties of homogeneous turbulent shear flow as well as the return to isotropy from anisotropic states due to shear and initially imposed polarization anisotropy. The anisotropy properties are quantified using the Reynolds stress anisotropy tensor and a wavelet-based scale-dependent decomposition of the velocity fields is used to compute the Reynolds stress anisotropy tensor at different scales of the turbulent motion. For homogeneous turbulent shear flow, the largest contribution to anisotropy originates at the larger scales of the turbulent motion. The smaller scales, however, are observed to show small levels of anisotropy. The return towards isotropy from anisotropic states due to shear and polarization anisotropy is strongest at the smallest scales of the turbulent motion, while anisotropy persists for multiple eddy-turnover time scales at the larger scales of the turbulent motion.

INTRODUCTION

The return to isotropy of anisotropic turbulence is of fundamental interest to understand turbulence dynamics and it has been studied and modelled in previous studies. Lumley & Newman (1977) considered the return to isotropy of homogeneous anisotropic turbulence without mean velocity gradients, drawing on previous work by Rotta (1951), Uberoi (1956, 1957), Mills & Corrsin (1959), and others. Choi & Lumley (2001) revisited the topic and analyzed results of three anisotropic flows. They observed that “the rate of return to isotropy was much lower for turbulence with a greater third invariant of the anisotropy tensor” and that the “turbulence wanted to become axisymmetric even more than it wanted to return to isotropy.” More recently, Briard *et al.* (2016) derive a model for the slow-part of the pressure-strain tensor to describe the return to isotropy and propose a decay law for anisotropic quantities in Batchelor turbulence. Yang *et al.* (2021) also consider the return to isotropy from homogeneous turbulent shear flows.

SIMULATIONS AND SCALE DECOMPOSITION

A number of direct numerical simulations of homogeneous turbulence are performed to study the anisotropy properties of homogeneous turbulent shear flow as well as the return to isotropy from its anisotropic state.

Numerical Approach

The coordinates $\mathbf{x} = (x, y, z) = (x_1, x_2, x_3)$ are directed in the downstream, vertical, and spanwise directions, respectively. In the case of shear, the downstream component of the mean velocity $\mathbf{U} = (U, V, W)$ has an imposed constant gradient $S = \partial U / \partial y$ in the vertical direction y :

$$U = Sy \quad V = W = 0 \quad (1)$$

This study is based on the Navier–Stokes equations for incompressible flow. This results in the following equation of motion for the fluctuating velocity components $\mathbf{u} = (u, v, w) = (u_1, u_2, u_3)$ and pressure p :

$$\nabla \cdot \mathbf{u} = 0 \quad (2)$$

$$\frac{\partial \mathbf{u}}{\partial t} + \mathbf{u} \cdot \nabla \mathbf{u} + Sy \frac{\partial \mathbf{u}}{\partial x} + Sv \mathbf{e}_x = -\frac{1}{\rho_0} \nabla p + \nu \nabla^2 \mathbf{u} \quad (3)$$

Here, ρ_0 the density, and ν the kinematic viscosity. The unit vector in the downstream direction is denoted as \mathbf{e}_x .

The equations of motion are transformed into a frame of reference moving with the mean velocity (Rogallo, 1981). This transformation enables the application of periodic boundary conditions for the fluctuating components of velocity and pressure. A spectral collocation method is used for the spatial discretization and the solution is advanced in time with a fourth-order Runge–Kutta scheme. The simulations are performed in a cubic computational domain of size $L_0^3 = (2\pi)^3$ using 512^3 grid points. In the cases without shear, we have $S = 0$ and $U = 0$.

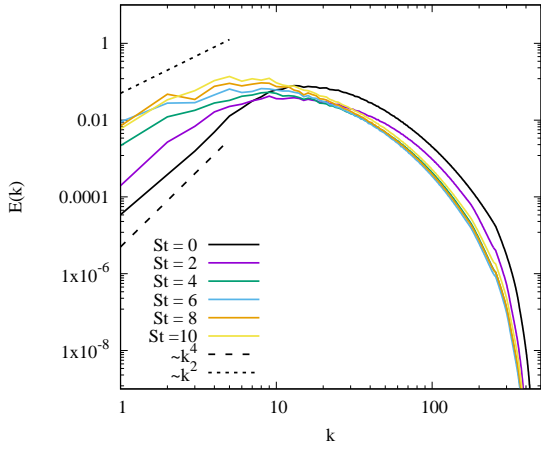


Figure 1. Evolution in non-dimensional time St of the energy spectrum $E(k)$ for homogeneous turbulent shear flow.

The initial conditions are taken from a separate simulation of isotropic turbulence. This simulation was initialized with random fluctuations with an imposed energy spectrum $E(k) \sim k^4$ for small wave numbers (Batchelor turbulence, see Batchelor & Proudman (1956)) and an energy density maximum at $k = 13$ in order to allow for growth of the large scales. The turbulence was allowed to develop for approximately one eddy turnover time and the k^4 dependence at small wave numbers was maintained. The resulting initial value of the Taylor-microscale Reynolds number is $Re_\lambda = q\lambda/v = 87$ and, in the case of turbulent shear flow, $SK/\varepsilon = 2$ for the shear number. Here $q = \langle u_i u_i \rangle^{1/2}$ is the magnitude of the velocity fluctuations, $K = q^2/2$ the turbulent kinetic energy, and $\varepsilon = \nu \langle \partial u_i / \partial u_k \partial u_k \partial u_i / \partial u_k \rangle$ its dissipation rate. The brackets $\langle \cdot \rangle$ denote a volume average at a fixed time, which is an appropriate choice for homogeneous flows.

The anisotropy of the flow is quantified using the Reynolds stress anisotropy tensor b_{ij} :

$$b_{ij} = \frac{\langle u_i u_j \rangle}{\langle u_k u_k \rangle} - \frac{1}{3} \delta_{ij} \quad (4)$$

Here, δ_{ij} is the Kronecker delta. This measure of the

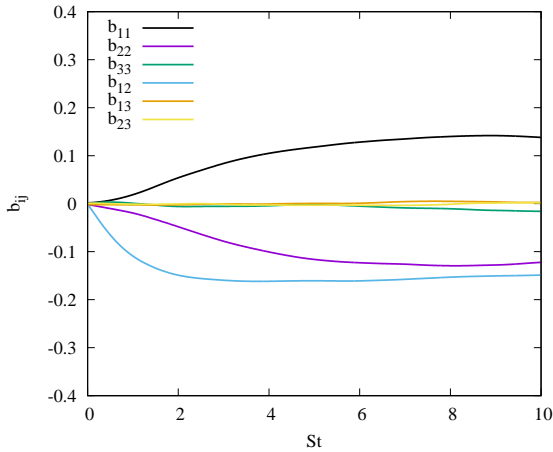


Figure 2. Evolution of the components of the Reynolds stress anisotropy tensor b_{ij} for homogeneous turbulent shear flow.

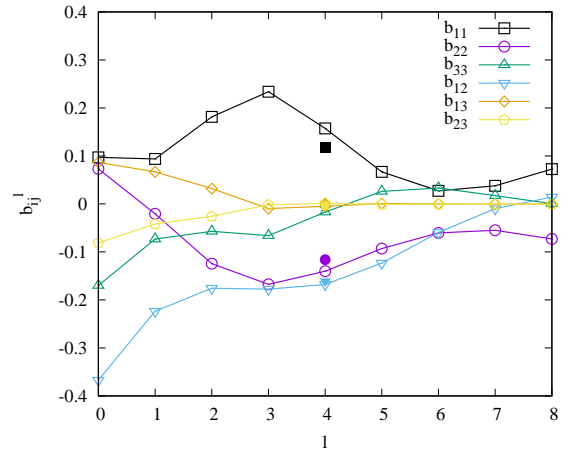


Figure 3. Scale decomposition of the components of the Reynolds stress anisotropy tensor b_{ij} for homogeneous turbulent shear flow at $St = 5$.

anisotropy was chosen due to its direct connection to the Reynolds stresses present in the flows.

Wavelet-Based Scale-Dependent Decomposition

A three-dimensional orthogonal vector-valued wavelet decomposition is used for defining scale-dependent statistics of different flow quantities. For reviews on wavelets in fluid mechanics we refer to Farge (1992) as well as Schneider & Vasilyev (2010). We consider a generic vector field $\mathbf{u} = (u_1, u_2, u_3)$ at a fixed time instant and decompose each component $u_\alpha(\mathbf{x})$ into an orthogonal wavelet series,

$$u_\alpha(\mathbf{x}) = \sum_{\lambda} \tilde{u}_{\lambda}^{\alpha} \psi_{\lambda}(\mathbf{x}). \quad (5)$$

The wavelet coefficients are given by the scalar product $\tilde{u}^{\alpha} = \langle u_{\alpha}, \psi_{\lambda} \rangle$ (e.g., Farge & Schneider, 2015). The wavelets ψ_{λ} with the multi-index $\lambda = (l, \mathbf{i}, d)$ are well localized in scale $L_0 2^{-l}$ (where L_0 corresponds to the size of the computational domain), around position $L_0 \mathbf{i} / 2^l$, and orientated in one of the

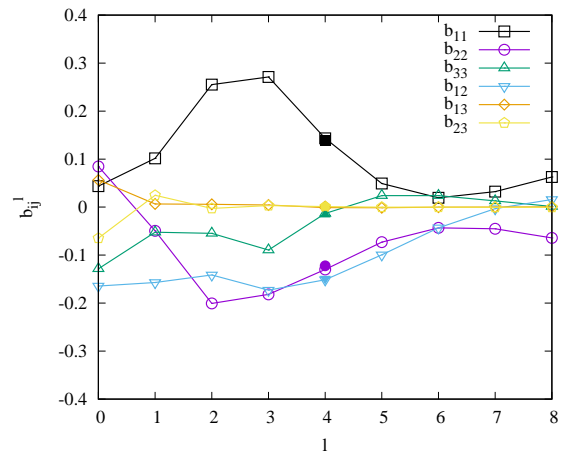


Figure 4. Scale decomposition of the components of the Reynolds stress anisotropy tensor b_{ij} for homogeneous turbulent shear flow at $St = 10$.

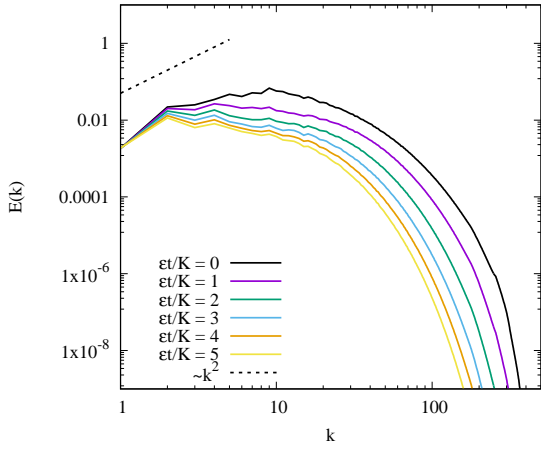


Figure 5. Evolution of the energy spectrum $E(k)$ towards return to isotropy started from homogeneous turbulent shear flow at $St = 5$.

seven directions $d = 1, \dots, 7$, respectively. The three components u_α at scale $L_0 2^{-l}$ can be reconstructed by summing only over the position i and direction d indices in eq. (5). The result yields the vector field \mathbf{u}^l at scale $L_0 2^{-l}$. Summing all scale contributions yields the total vector field, $\mathbf{u} = \sum_l \mathbf{u}^l$, as the \mathbf{u}^l are mutually orthogonal.

The scale-dependent statistical moments of the flow fields can thus be computed from \mathbf{u}^l using classical statistical estimators. For instance, the scale-dependent components of the Reynolds stress anisotropy tensor can be defined as follows:

$$b_{ij}^l = \frac{\langle u_i^l u_j^l \rangle}{\langle u_k^l u_k^l \rangle} - \frac{1}{3} \delta_{ij} \quad (6)$$

RESULTS

In the following, the anisotropy properties of homogeneous turbulent shear flow, initialized with an isotropic turbulence field, are presented first at two different times $St = 5$ and $St = 10$. The anisotropic flow fields at $St = 5$ and $St = 10$

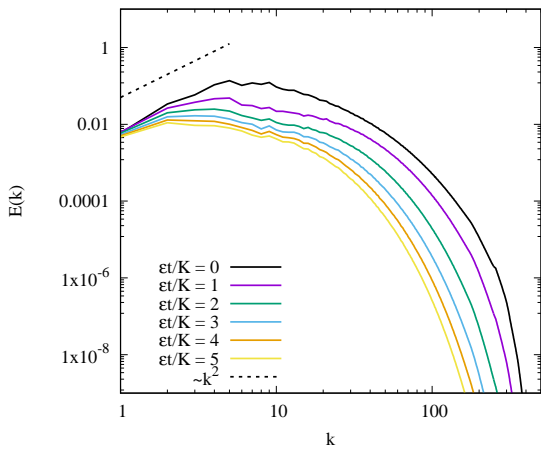


Figure 6. Evolution of the energy spectrum $E(k)$ towards return to isotropy started from homogeneous turbulent shear flow at $St = 10$.

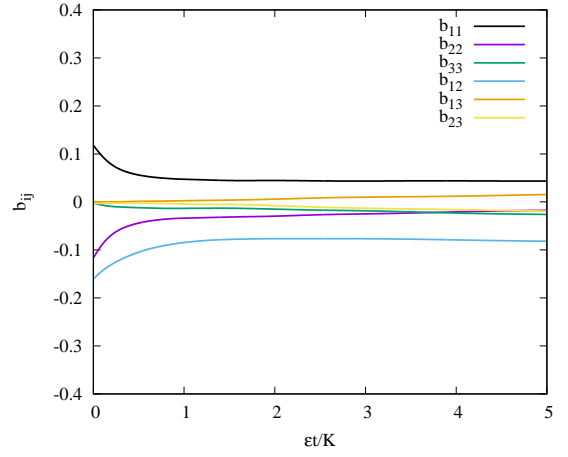


Figure 7. Evolution of the components of the Reynolds stress anisotropy tensor b_{ij} towards return to isotropy started from homogeneous turbulent shear flow at $St = 5$.

are then used to study the return towards isotropy without the mean velocity gradient. Additionally, polarization anisotropy is imposed on the original isotropic turbulence field, resulting in an anisotropic field, and its return toward isotropy is considered.

Homogeneous Turbulent Shear Flow

Starting with the initial condition described above, a simulation of homogeneous turbulent shear flow was carried out. After an initial decay of the turbulent kinetic energy $K = \overline{u_i u_i} / 2$ due to the isotropic initial condition, anisotropy develops at approximately nondimensional time $St = 2$, production of K sets in, and the turbulent kinetic energy eventually grows exponentially. At the end of the simulation at $St = 10$, the Taylor-microscale Reynolds number reaches a value of $Re_\lambda = 128$ and the shear number assumes an approximately constant value of $SK/\varepsilon = 5$.

The evolution of the spherically averaged energy spectrum $E(k)$ is shown in figure 1. The spectrum at $St = 0$ shows the isotropic initial condition with a Batchelor spectrum $E(k) \sim k^4$ for small wave numbers. During the initial isotropic decay until about $St = 2$, the energy spectrum de-

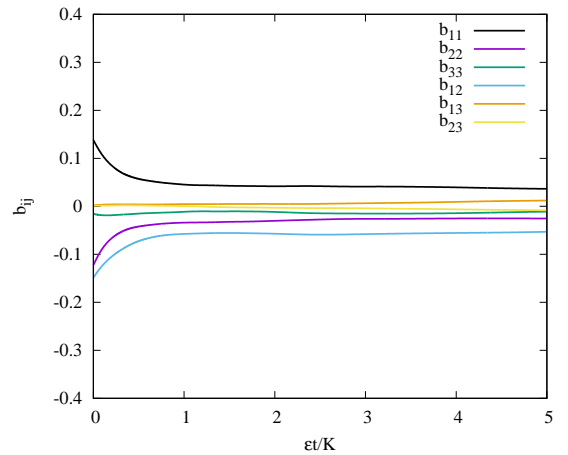


Figure 8. Evolution of the components of the Reynolds stress anisotropy tensor b_{ij} towards return to isotropy started from homogeneous turbulent shear flow at $St = 10$.

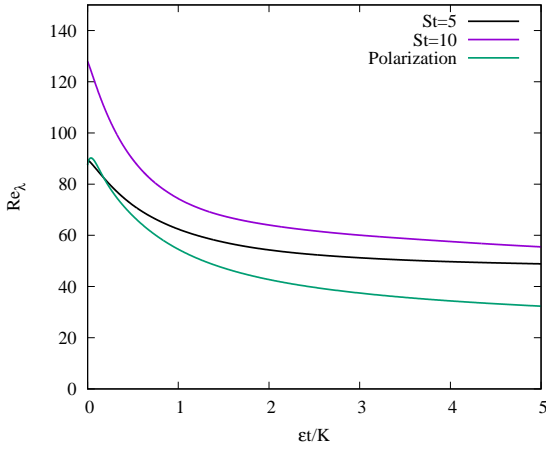


Figure 9. Evolution of the Taylor micro-scale Reynolds number Re_λ .

cays for wave numbers $k \gtrsim 10$ and grows for $k \lesssim 10$, and for which the Batchelor spectrum approximately persists. The anisotropy strongly increases until about $St = 4$. During this period of the flow evolution, the energy spectrum continues to decrease for larger $k \gtrsim 12$, grows for smaller wave numbers, and the spectral slope at the smallest wave numbers decreases. For $St \gtrsim 4$, the turbulence has reached its eventual state (exponential growth of K , see Jacobitz *et al.* (1997)) with energy growth at small wave numbers and an energy spectrum $E(k) \sim k^2$ for small wave numbers (Saffman turbulence, see Saffman (1967)). A Saffman type spectrum at low wave numbers was also observed for forced isotropic turbulence by Alexakis & Brachet (2019).

The development of the components of the Reynolds shear stress anisotropy tensor b_{ij} in non-dimensional time St is shown in figure 2. The diagonal components eventually reach approximately constant values with $b_{11} > b_{33} > b_{22}$ or downstream > cross-stream > vertical. The off-diagonal component b_{12} develops quickly and it determines the timing of the spectral flow development described above. The remaining two off-diagonal components remain small. More details of the anisotropy properties of homogeneous turbulent shear flow, including the effects of rotation, can be found in Jacobitz *et al.* (2010) and Salhi *et al.* (2014).

The wavelet-based scale-dependent decomposition of the components of the Reynolds stress anisotropy tensor b_{ij}^l are shown in figures 3 for $St = 5$ and 4 for $St = 10$. The figures show the dependence of the b_{ij}^l components (open symbols) on the scale index l with small l corresponding to the large scales of the turbulent motion and large l corresponding to the small scales. Additionally, the b_{ij} components for the total fields (filled symbols) are also shown in the center of the graphs. At both times, strong anisotropy b_{ij}^l is observed at the large scales of the turbulent motion with scale index $l \lesssim 4$. Often, but not always, the observed b_{ij}^l at the large scales exceed the b_{ij} obtained for the total fields. Please note that the decomposed fields for the smallest scale indices $j = 0$ and $j = 1$ are based on very few wavelet modes and may not result in reliable statistics. At both times, smaller anisotropy b_{ij}^l is observed at the large scales of the turbulent motion with $l \gtrsim 5$. However, some components of b_{ij}^l remain clearly non-zero at the smallest scales of the turbulent motion.

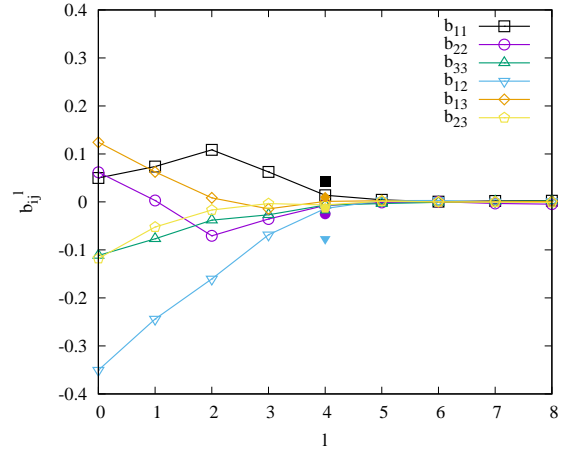


Figure 10. Scale decomposition of the components of the Reynolds stress anisotropy tensor b_{ij} towards return to isotropy started from homogeneous turbulent shear flow at $St = 5$. The scale decomposition is shown after a return towards isotropy for three eddy-turnover times.

Return to Isotropy from Homogeneous Turbulent Shear Flow

The homogeneous turbulent shear flow results at non-dimensional times $St = 5$ and $St = 10$ with developed anisotropy are allowed to return towards isotropy. The time $St = 5$ was chosen as the Reynolds number $Re_\lambda = 89$ is close to the value of the original isotropic turbulence initial condition. The Reynolds number at time $St = 10$ has increased to a value $Re_\lambda = 128$. The flow is allowed to decay towards isotropy for five eddy turnover times.

Figures 5 and 6 show the development of the energy spectra for the two cases as et/K time progresses. In both cases, a decay of the energy is observed at all wave numbers and the Saffman type spectrum established during the shear forcing of the previous simulation persists at low wave numbers.

The evolution of the components of Reynolds stress anisotropy tensor b_{ij} in non-dimensional time et/K are shown in figures 7 and 8. In both cases, the non-zero components

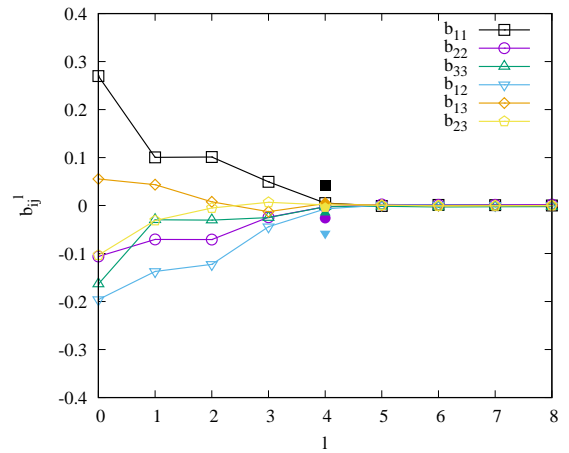


Figure 11. Scale decomposition of the components of the Reynolds stress anisotropy tensor b_{ij} towards return to isotropy started from homogeneous turbulent shear flow at $St = 10$. The scale decomposition is shown after a return towards isotropy for three eddy-turnover times.

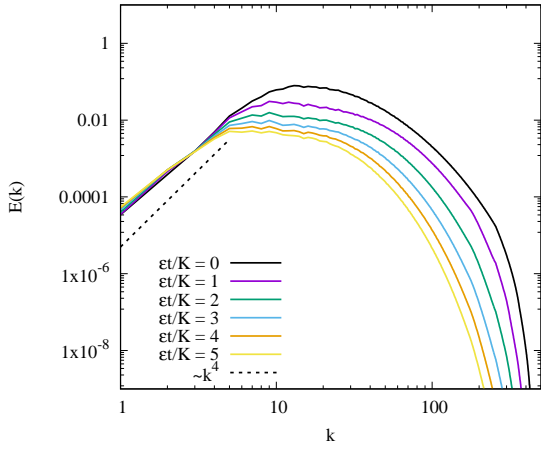


Figure 12. Evolution of the energy spectrum $E(k)$ towards return to isotropy started from homogeneous isotropic turbulence with imposed polarization anisotropy.

b_{11} , b_{22} , and b_{12} show a strong decay towards isotropy for about one eddy-turnover. Similar to the observations in Choi & Lumley (2001), the decay then slows. The initially zero components even develop a low level of anisotropy. Figure 9 shows the evolution of Reynolds number Re_λ in non-dimensional time $\epsilon t/K$. The Reynolds number also shows a strong decrease for about one eddy-turnover.

Figures 10 and 11 present the wavelet-based scale-dependent decomposition of the components of the Reynolds stress anisotropy tensor b_{ij}^l for the two cases at non-dimensional time $\epsilon t/K = 3$. For both cases, strong anisotropy persists at the large scales of the turbulent motion with scale index $l \lesssim 4$. However, a return to isotropy is observed for both cases at the small scales of the turbulent motion with scale index $l \gtrsim 5$.

Return to Isotropy from Polarization Anisotropy

The results of a return to isotropy from an anisotropic homogeneous turbulent shear flow presented in the previous section, are now compared to results of a return to isotropy sim-

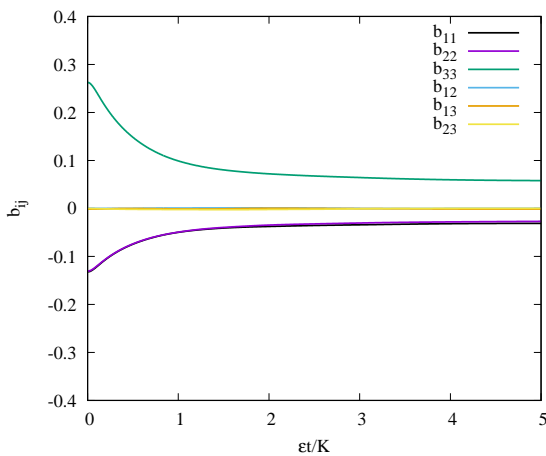


Figure 13. Evolution of the components of the Reynolds stress anisotropy tensor b_{ij} towards return to isotropy started from homogeneous isotropic turbulence with imposed polarization anisotropy.

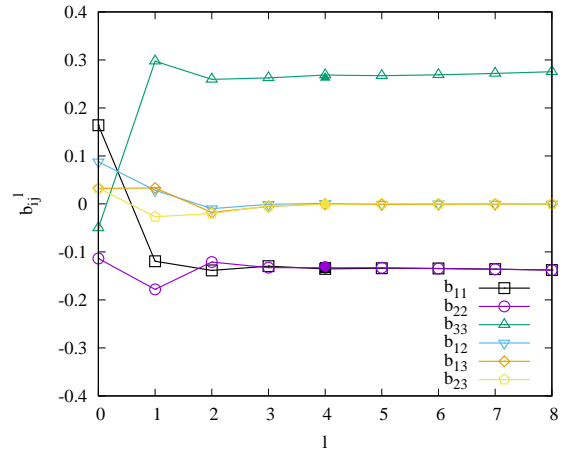


Figure 14. Scale decomposition of the components of the Reynolds stress anisotropy tensor b_{ij} towards return to isotropy started from homogeneous isotropic turbulence with imposed polarization anisotropy at $\epsilon t/K = 0$.

ulation, which is initialized with polarization anisotropy. Following the approach given in Morinishi *et al.* (2001) or Cambon *et al.* (1992), polarization anisotropy is imposed by linking the complex conjugate coefficients in helical wave space with a constant phase angle $\Phi_0 = 0$. This results in an anisotropic turbulence field with $b_{11} = b_{22} = -1/2b_{33}$.

Figure 12 shows the decay towards isotropy of the energy spectrum $E(k)$ with non-dimensional time $\epsilon t/K$. The decay is observed at all wave numbers $k \gtrsim 5$, while the largest wave numbers approximately retain their Batchelor type spectrum $\sim k^4$.

The evolution of the components of the Reynolds shear stress anisotropy tensor b_{ij} is shown in figure 13. The non-zero diagonal components b_{11} , b_{22} , and b_{33} again show a strong decay towards isotropy for about one eddy turnover. After that, the decrease slows considerably, similarly to the decrease of the Reynolds number Re_λ as shown in figure 9. The off-diagonal components remain small.

The wavelet-based scale-dependent decomposition of the components of the Reynolds stress anisotropy tensor b_{ij}^l are

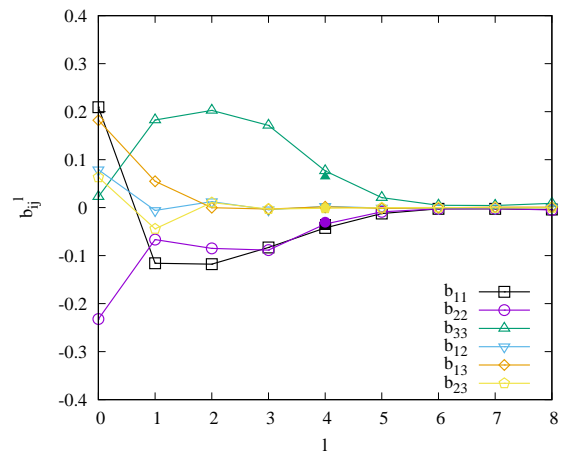


Figure 15. Scale decomposition of the components of the Reynolds stress anisotropy tensor b_{ij} towards return to isotropy started from homogeneous isotropic turbulence with imposed polarization anisotropy at $\epsilon t/K = 3$.

shown in figures 14 for $\epsilon t/K = 0$ and 15 for $\epsilon t/K = 3$. The polarization anisotropy imposed on an originally isotropic turbulence field results in approximately constant anisotropy for the diagonal components of b_{ij}^l at all scale indices l . Exceptions are the smallest scale indices $l = 0$ and $l = 1$, which are computed from a small number of modes in wavelet space. As time progresses and the turbulence decays, strong anisotropy b_{ij}^l remains present in the turbulent fields at the large scales of the turbulent motion with scale index $l \lesssim 4$. Again, the observed b_{ij}^l values at the large scales with $1 \leq l \leq 4$ exceed the b_{ij} obtained for the total fields. As in previous return to isotropy cases, only very small levels of anisotropy b_{ij}^l are observed at the small scales of the turbulent motion with $l \gtrsim 5$.

SUMMARY

The anisotropy properties of homogeneous turbulent shear flow as well as the return to isotropy from anisotropic states due to shear and initially imposed polarization anisotropy is studied using results from direct numerical simulations. The velocity fields of the turbulent fluctuations are decomposed by scale using a wavelet-based approach. The components of the Reynolds stress anisotropy tensor are then calculated at different scales of the turbulent motion as well as for the total fields. For homogeneous turbulent shear flow, strong anisotropy is observed at the larger scales of the turbulent motion, while lower levels of anisotropy are also obtained at the smaller scales of the turbulence. A complete return to isotropy is observed within about one eddy-turnover time for cases initialized with anisotropic states due to shear at two different Reynolds numbers and due to imposed polarization anisotropy for the smaller scales of the turbulent motion. However, anisotropy persists for multiple eddy-turnover time scales at the larger scales of the turbulent motion. This observation could be due to the decrease of the Reynolds number as time progresses. Future work will address the effect of Reynolds number as well as consider a similar series of simulations initialized with Saffman turbulence.

ACKNOWLEDGEMENTS

FGJ would like to acknowledge sabbatical leave support from the University of San Diego and a visiting position at Aix-Marseille University. KS acknowledges financial support from the French Federation for Magnetic Fusion Studies (FR-FCM) and the Eurofusion consortium, funded by the Euratom Research and Training Programme under Grant Agreement No. 633053. The views and opinions expressed herein do not necessarily reflect those of the European Commission. KS acknowledges partial funding from the Agence Nationale de la Recherche (ANR), project CM2E, grant ANR-20-CE46-0010-01.

REFERENCES

- Alexakis, A. & Brachet, M.-E. 2019 On the thermal equilibrium state of large-scale flows. *J. Fluid Mech.* **872**, 594–625.
- Batchelor, G. K. & Proudman, I. 1956 The large-scale structure of homogenous turbulence. *Philos. Trans. R. Soc. A* **248** (949), 369–405.
- Briard, A., Gomez, T., Mons, V. & Sagaut, P. 2016 Decay and growth laws in homogeneous shear turbulence. *J. Turbul. Fluids A-Fluid* **17** (7), 699–726.
- Cambon, C., Jacquin, L. & Lubrano, J. L. 1992 Toward a new Reynolds stress model for rotating turbulent flows. *Phys. Fluids A-Fluid* **4** (4), 812–824.
- Choi, K.-S. & Lumley, J. L. 2001 The return to isotropy of homogeneous turbulence. *J. Fluid Mech.* **436**, 59–84.
- Farge, M. 1992 Wavelet transforms and their applications to turbulence. *Annu. Rev. Fluid Mech.* **24** (1), 395–458.
- Farge, M. & Schneider, K. 2015 Wavelet transforms and their applications to mhd and plasma turbulence: a review. *J. Plasma Phys.* **81** (6), 435810602.
- Jacobitz, F. G., Sankar, S. & Van Atta, C. W. 1997 Direct numerical simulations of the turbulence evolution in a uniformly sheared and stably stratified flow. *J. Fluid Mech.* **342**, 231–261.
- Jacobitz, F. G., Schneider, K., Bos, W. J. T. & Farge, M. 2010 On the structure and dynamics of sheared and rotating turbulence: Anisotropy properties and geometrical scale-dependent statistics. *Phys. Fluids* **22** (8).
- Lumley, J. L. & Newman, G. R. 1977 The return to isotropy of homogeneous turbulence. *J. Fluid Mech.* **82** (1), 161–178.
- Mills, R. R. & Corrsin, S. 1959 Effect of contraction on turbulence and temperature fluctuations generated by a warm grid. *Tech. Rep.*
- Morinishi, Y., Nakabayashi, K. & Ren, S. Q. 2001 Dynamics of anisotropy on decaying homogeneous turbulence subjected to system rotation. *Phys. Fluids* **13** (10), 2912–2922.
- Rogallo, R. S. 1981 Numerical experiments in homogeneous turbulence. Technical Report TM 81315. NASA Ames Research Center, Moffett Field, CA, United States.
- Rotta, J. C. 1951 Statistische Theorie nichthomogener Turbulenz. *Z. Phys.* **129**, 547–572.
- Saffman, P. G. 1967 The large-scale structure of homogeneous turbulence. *J. Fluid Mech.* **27** (3), 581–593.
- Salhi, A., Jacobitz, F. G., Schneider, K. & Cambon, C. 2014 Nonlinear dynamics and anisotropic structure of rotating sheared turbulence. *Phys. Rev. E* **89** (1), 013020.
- Schneider, K. & Vasilyev, O. V. 2010 Wavelet methods in computational fluid dynamics. *Annu. Rev. Fluid Mech.* **42**, 473–503.
- Uberoi, M. S. 1956 Effect of wind-tunnel contraction on free-stream turbulence. *J. Aeronaut. Sci.* **23** (8), 754–764.
- Uberoi, M. S. 1957 Equipartition of energy and local isotropy in turbulent flows. *J. Appl. Phys.* **28** (10), 1165–1170.
- Yang, P.-F., Pumir, A. & Xu, H. 2021 Return to isotropy of homogeneous shear-released turbulence. *Phys. Rev. Fluids* **6** (4), 044601.